Enceladus Orbilander: A Mission Concept Study to Search for Signs of Life

S. M. MacKenzie[1]*, M. Neveu[2], A.F. Davila[3], J.I. Lunine[4], K.L. Craft[1], M.L. Cable[5], J.L. Eigenbrode[2], R. Gold[1], C.M. Phillips-Lander[6], J.D. Hofgartner[5], J.H. Waite[6], C.R. Glein[6], C.P. McKay[3] and the Orbilander Team

[1]Johns Hopkins Applied Physics Lab, [2]NASA GSFC, [3]NASA Ames, [4]Cornell University, [5]JPL Caltech, [6]SwRI, *shannon.mackenzie@jhuapl.edu

APL Johns Hopkins Applied Physics Laboratory

Science Objectives

Science		Feature of Life (from Neveu et al. 2018) or Environment	Measurement	Rationale (Biosignature/Interpretation)
Ques.	Objective			
Is Enceladus inhabited?	1. Characterize the bulk organic fraction of volatile and non-volatile plume materials	Potential biomolecule components	1A. Molecular weight distribution of organic matter from 16 Da (CH_4) to ≥1000 Da in plume vapor and icy particles 1B. Relative abundance and diversity of organic functional groups, including whole molecules, molecular fragments and compounds potentially indicative of life such as hopanes 1C. 13C/12C abundances of CO_2, CO, and CH_3-type molecular fragments released by heating sampled material at different temperatures	A. Molecular Assembly Index: distribution of the number of types of operations needed to obtain each molecule in the pool of detected organic compounds (Marshall et al., 2021) B. Chemical Context: Inventory of organic chemical species, including specific functional groups, in the context of known biotic and abiotic distributions C. Isotope Patterns: isotopes become unevenly distributed due to biological and abiotic processes in ways that inform the history and provenance of the material (Hinrichs et al., 2001)
	2. Characterize the amino-acid composition of plume materials	Potential biomolecule components	2A. Relative abundances of amino acid (a.a.) isomers, including at least Gly and four of: Ala, Asp, Glu, His, Leu, Ser, Val, Iva, β-Ala, γ-aminobutyric acid, and aminoisobutyric acid, with at least one abiotic and biotic representative, at accuracy ≤ 10%	Use Gly abundance to normalize other abundances: Gly is the smallest a.a. and the most common in abiogenic meteoritic samples (Creamer et al., 2017). Aminoisobutyric acid is abiotic, rare on Earth, but abundant in some carbonaceous meteorites (Glavin et al., 2020). β-Ala and γ-aminobutyric acid are found in biology as metabolic intermediates but are not used to build proteins (Glavin et al., 2020). The other amino acids are proteinogenic and expected in higher abundance relative to Gly in biogenic samples compared to abiogenic samples. A 10% relative uncertainty enables clear distinction between biotic and abiotic distributions (Creamer et al., 2017).
		Enantiomeric excess	2B. Relative abundances of L- and D-enantiomers of a.a. with molecular mass b/w D/L-Ala (71 Da) and D/L-Glu (129 Da), including ≥2 among Ala, Val, and β-amino-n-butyric acid; ≥3 proteinogenic; 1 abiotic a.a.; and histidine at accuracy ≤ 10%	Ala, Val, and β-amino-n-butyric acid are usually present as racemic or near-racemic mixtures in meteorites and other abiotic systems (Glavin et al., 2012, 2020). Histidine has not been found abiotically (Glavin et al., 2020).
	3. Characterize the lipid composition of plume materials	Potential biomolecule components	3A. Relative abundances, composition, and commonalities of compounds that define subsets of long-chain aliphatic hydrocarbons (e.g., carboxylic acids, fatty acids, (un)saturated hydrocarbon chains) up to 500 Da at accuracy ≤ 20%	Distribution abundance pattern as a function of carbon chain-length; patterns in molecular size distributions (e.g. limited carbon chain length range) (Summons et al., 2008).
	4. Search for evidence of a genetic biopolymer in plume materials	Functional molecules and structures	4A. Presence of a polyelectrolyte (polymer with a repeating charge in its backbone)	A linear polymer with repeating charge could be a universal feature of life, indicative of a biological entity capable of Darwinian evolution (Benner, 2017). This can also be used as a terrestrial contamination test, for example, by looking for DNA sequences of microorganisms common in clean rooms.
	5. Search for evidence of cells in plume materials	Cells	5A. Morphology (size, shape, and aspect ratio) of non-icy particles as small as 0.2 μm in diameter. 5B. Organic content (e.g., native autofluorescence) associated with non-icy particles	Morphologies resembling cells colocated with physical activity (e.g., motion), chemical activity, or biocompositional features
To what extent is Enceladus' ocean able to sustain life and why?	6-7. Determine the physical/chemical environment of the ocean	Ocean pH	6.1A. Hydrogen ion concentration	Direct measurement
			6.1B. Abundances of CO_2, and bicarbonate or carbonate; relative abundances of all organic and inorganic species (e.g. Cl-containing compounds, carbonates, sulfates, metal hydroxides, silica, and silicates)	pH Derived from relative abundances of CO_2, and bicarbonate or carbonates in the plume (Glein et al., 2015)
		Ocean temperature	6.2A. Relative abundances of D/H of H_2, D/H of H_2O, and ethylene/ethane 6.2B. Relative abundances of bulk organic and inorganic species (e.g. Cl-containing compounds, carbonates, sulfates, metal hydroxides, silica, and silicates) with masses ≤ 500 Da	A. Derived from geothermometer species (Proskurowski et al., 2006; Fiebig et al., 2013) B. Infer possible reaction temperatures from high-mass species and silica concentration (e.g., Sekine et al., 2015)
		Ocean salinity	6.3A. Conductivity of plume materials 6.3B. Abundance of Na, Cl ions	A. Direct measurement B. Direct measurement. Na and Cl appear to dominate Enceladus' salt abundances (e.g., Postberg et al., 2018b).
		Sources of nutrients and energy	6.4A. Presence and relative abundances of CHNOPS-bearing compounds (including H_2) in plume materials and other micronutrients (e.g. Ca, Mg, and Fe) 6.4B. Redox potential (Eh) 6.4C. Abundances of oxidants (e.g. SO_4^{2-}, CO_2 or HCO_3^-, NO_3^-, O_2) and reductants (e.g. H_2S, CH_4, NH_3 or NH_4^+, H_2) 6.4D. Presence and relative abundances of products of radiolytic decomposition of surface water ice (e.g. OH^-, H_2O_2)	A. Direct measurement. Cassini detected all but P,S. B. Inferred from presence and abundance of redox-active species. C-D. Constrains redox disequilibria due to products of radiolytic decomposition of surface ice (McCollom and Shock, 1997) by comparing plume abundances to surface deposits (Ray et al., 2020).
		Structure, dynamics, and evolution of the interior	7A. Body-wave arrival times 7B. Tide-induced displacement 7C. Free oscillations	Seismic sources are expected to abound on Enceladus' fractured south polar terrain, which experiences cryovolcanism and tidal flexing (e.g., Kite & Rubin, 2016; Běhounková et al., 2017). Monitoring seismic waves propagated through Enceladus' interior and along its surface probes its interior structure (ice thickness, ocean depth, core size and mechanical properties, ocean stratification if any), surface and shallow fracturing due to tidal flexing, and associated tidal periodicities, informing the properties and processes affecting ocean samples along their path to the plume (Vance et al., 2018).
			7D. Abundances of noble gases (especially 40 Ar), K, D/H, and 16O/18O	Determine the abundance of radiogenic 40Ar to constrain its timescale of accumulation (Waite et al., 2009). The Cassini INMS measurement could not be reproduced in later observations due to both insufficient sensitivity and mass resolution to distinguish 40Ar from organic compound fragments. This also enables radiometric dating of plume material by concurrently measuring the plume K abundance (e.g., via MS) (Postberg et al., 2011). Expect a K-Ar age = solar system age, unless Enceladus rock experienced a more recent resetting (e.g. melting) event. Determine if noble gas abundances are similar to or distinct from those expected if trapping into clathrate hydrates occurs, informing the presence of clathrates and their ability to trap other volatiles (e.g., H_2, CO_2, CH_4) and affect the thermal and mechanical properties of the interior and the composition of the ocean (Bouquet et al., 2015).
	8.1. Characterize the structure and dynamics of the crust	Intracrust fluid reservoirs	8.1A1. Body wave coda, body and surface wave arrival times 8.1A2. Radargrams over SPT	A1. Used to determine speed of sound and any attenuation within the ice shell due to local fluid reservoirs; detect seismic sources due to fluid flow in the shell (Vance et al., 2018) A2. Dielectric changes indicative of compositional changes result in interfaces that reflect radar-emitted waves (Grima et al. 2016; Heggy et al., 2017)
		Regional crustal thickness	8.1B1. Surface wave dispersion curves, body and surface wave arrival times 8.1B2. Radargrams over SPT	B1. Seismic monitoring can be used to derive ice shell thickness variations of < 50 m with spatial resolution < 1 km (Vance et al., 2018) B2. Density changes indicative of compositional changes result in interfaces that reflect radar-emitted waves (Heggy et al., 2017)
		Regional topography and Love numbers	8.1C1. Limb profiles 8.1C2. Height of surface	Spatial & temporal variations of Enceladus' shape are essential in helping determine Enceladus' interior structure (Thomas et al., 2016; Hemingway & Mittal, 2019)
			8.1D. Love numbers, hi, h2, l2, and k2 to 0.1%	Temporal variations of Enceladus' shape and gravity constrain the mechanical properties of the interior (e.g., less et al., 2014; Hemingway & Mittal, 2019). Meaningful constraints can be derived with sub-percent precision on the Love numbers.
	8.2. Infer ascent and freezing conditions	Composition	8.2A. Composition of plume grains at various locations, altitudes, and mean anomalies.	Spatial & temporal variations in plume compositions constrain processes and conditions of eruption. The kinetics of freezing during ascent can influence composition (Thomas et al., 2019). The plume composition varies with tidal forcing (Hurford et al., 2007) and spatially (grain-to-gas ratio; Hedman et al., 2018), finer compositional variations remain to be elucidated.
		Rate of fallout	8.2B. Rate of plume material collected in orbit and on the surface	Quantify the mass of ejected material that cannot be sampled during fly-throughs.
	8.3. Determine the physical structure of the jet vent openings	Surface thermal properties	8.3A. Thermal emission spectra at wavelengths 10—50 μm	Map surface temperatures, surface heat flux, and determine the thermal properties of surface material from temperature variations (e.g., Howett et al., 2011).
		Vent morphology and topography	8.3B. Surface topography near the vents at sub-meter horizontal, 10-cm vertical resolution	The topography near vents informs their shape and thus conditions (e.g., temperature, pressure, velocity) encountered by ocean samples during ejection (Goldstein et al., 2018; Ono et al., 2019)
			8.3D. Horizontal and vertical surface displacement at sub-meter spatial resolution, 10-cm vertical resolution	Tidally modulated vent eruptions (Hurford et al., 2007; Goldstein et al., 2018) expected to result in m-scale displacement (Běhounková et al., 2017) quantifiable with dm-scale resolution.
		Subsurface structure	8.3C. Location and extent of liquid-filled pockets in the south polar terrain	See 8.1A

Payload

The science objectives above were traced to an example payload of candidate instruments. Other instruments and investigation could be considered.

Not shown is the Sampling Suite, which is critical to successful LDS measurements:

(1) collects sample
(2) delivers sample to the central processing unit
(3) processes the sample for each instrument
(4) delivers sample to instruments
(5) flushes the system clean for the next analysis

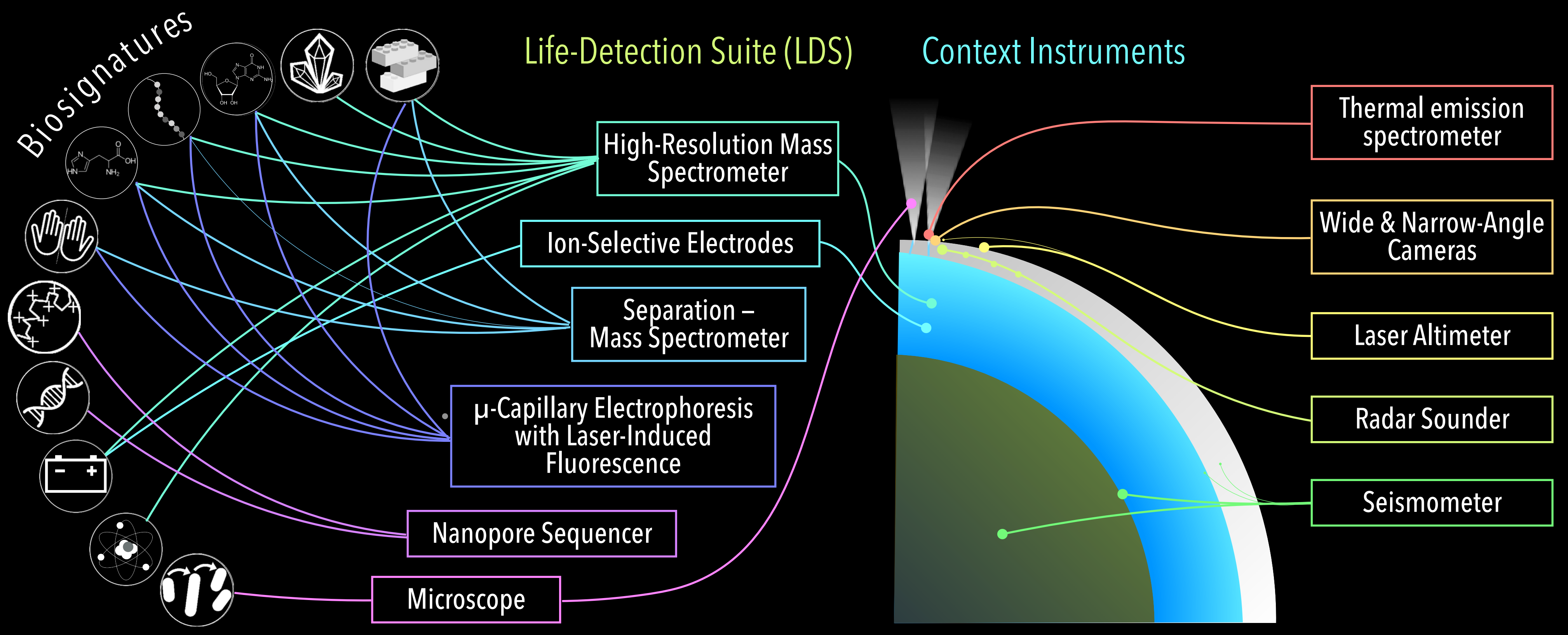

Mission Overview

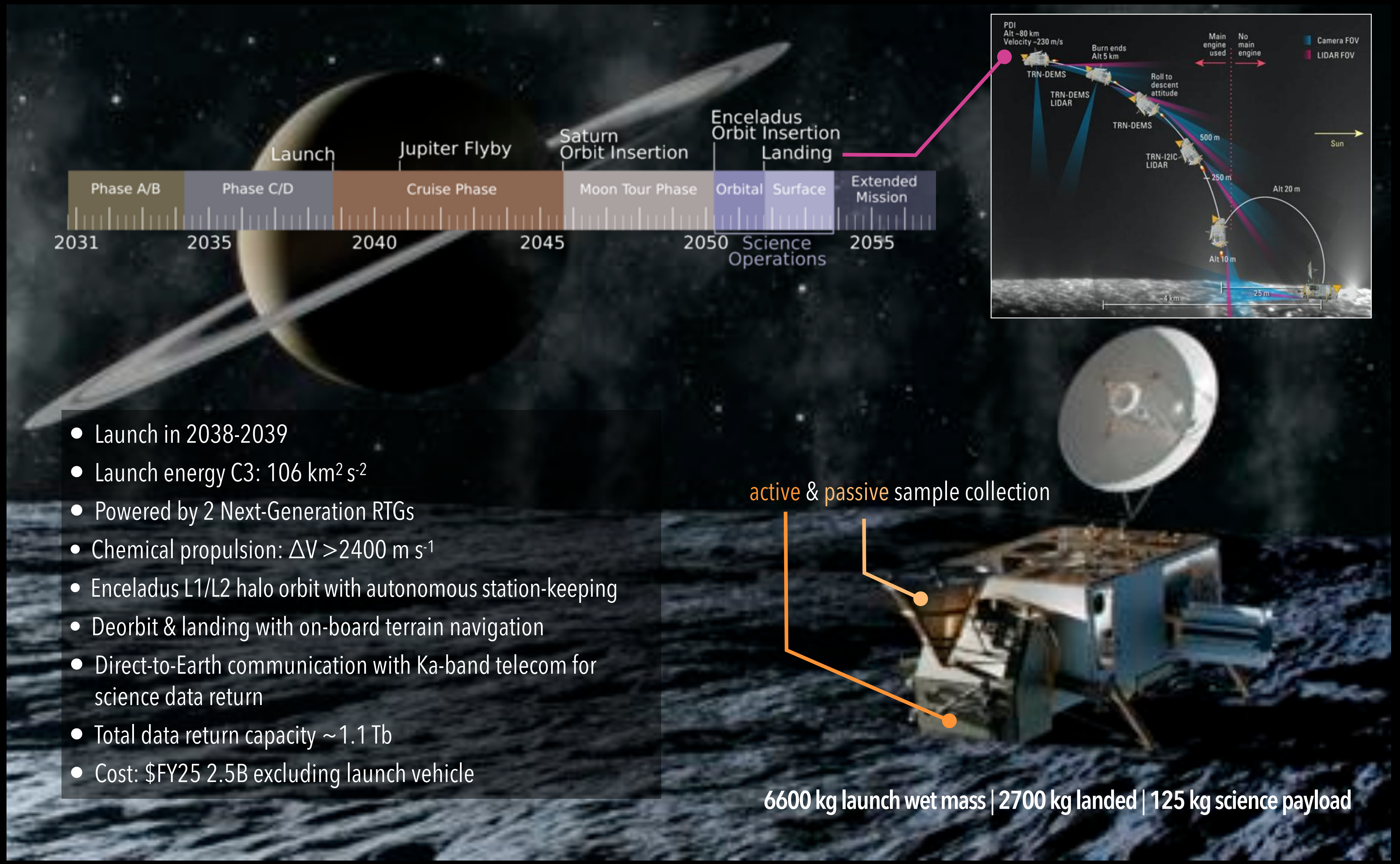

- Launch in 2038-2039
- Launch energy C3: 106 $km^2 s^{-2}$
- Powered by 2 Next-Generation RTGs
- Chemical propulsion: $\Delta V > 2400$ m s^{-1}
- Enceladus L1/L2 halo orbit with autonomous station-keeping
- Deorbit & landing with on-board terrain navigation
- Direct-to-Earth communication with Ka-band telecom for science data return
- Total data return capacity ~1.1 Tb
- Cost: $FY25 2.5B excluding launch vehicle

Concept of Operations